

Decaying fermionic warm dark matter and XENON1T electronic recoil excess

Koushik Dutta,^{1,*} Avirup Ghosh,^{2,†} Arpan Kar,^{2,‡} and Biswarup Mukhopadhyaya^{1,§}¹*Department of Physical Sciences, Indian Institute of Science Education and Research, Kolkata, Mohanpur - 741246, India*²*Regional Centre for Accelerator-based Particle Physics, Harish-Chandra Research Institute, HBNI, Chhatnag Road, Jhansi, Allahabad - 211 019, India*

In the light of the recently observed XENON1T electronic recoil (ER) data, we investigate the possibility of constraining the parameter space of a generic fermionic warm dark matter (WDM), decaying into a standard model (SM) neutrino and a photon. The photon as a decay product, when produced inside the XENON1T chamber, interacts with an electron of a xenon (Xe) atom, leading to a contribution in the observed ER data. We add this dark matter (DM) induced signal over the standard background (B_0) considered by the XENON1T collaboration and perform a χ^2 fit against the XENON1T data to obtain the best-fit values of the DM decay width and the associated 95% confidence level (C.L.) band for DM mass (m_χ) varied in the range 2 – 60 keV. Additionally, we have extended our analysis by including two other background models available in the literature and in each case, the corresponding limits on the DM decay width are estimated for DM mass (m_χ) in the domain 2 – 18 keV. By comparing the constraints, obtained by fitting the XENON1T data, with the upper limits arising from various existing astrophysical and cosmological observations, we find that, for the background model B_0 , a fair amount of the DM parameter space is allowed at 95% C.L. for DM masses outside the range $3.5 \text{ keV} \lesssim m_\chi \lesssim 8.5 \text{ keV}$. However, in case of other two background models, reasonable parts of the DM parameter space are favoured at 95% C.L. by all astrophysical data for all DM masses in the range 2 – 18 keV.

Keywords: XENON1T, electronic recoil excess, decaying fermionic WDM, X-ray observations

I. INTRODUCTION

Recently, XENON1T has reported an excess in its electronic recoil (ER) events in the energy range 2 – 3 keV [1, 2]. Several scenarios have already been proposed in explaining this excess as potential signals of bosonic dark matter (DM) candidates [3–11], Primakoff process involving solar axions [12–16], neutrino magnetic moment [17–21] along with many other new physics possibilities [22–24]. In [25], a decaying fermionic warm dark matter (WDM) particle, which produces a dark photon, has been considered as a possible explanation. In most of these cases, the interactions which cause the XENON1T ER events are difficult to probe in indirect search observations. Some previous works [26–28] have also tried to fit the observed data using various possible background models (other than the standard background B_0 [1, 2]), leaving some small scopes for adding new signals.

In this paper, we assume a fermionic DM (χ) whose mass (m_χ) is in the keV range and which decays into a photon (γ) along with a SM neutrino (ν). It is a scenario studied in the past in several contexts [29–39]. One theoretical basis of such a possibility is offered by R-parity violating supersymmetry (SUSY) with a keV-scale warm dark matter candidate such as the gravitino or the axino [32–39]. The breakdown of R-parity (defined as $R = (-1)^{3B+L+2J}$) via bilinear L-breaking terms in the superpotential leads to photino-neutrino mixing. This

in turn can drive the decay of the gravitino/axino into a photon and a neutrino, with the photon in the right energy range answering to the XENON1T observation. Keeping this in mind, we perform a model-independent analysis, assuming tentatively that the keV-scale DM particle saturates the observed DM densities in the galaxies.

In this scenario, the local population of χ decays inside the XENON1T detector and the resulting photons contribute to the XENON1T ER events by means of photoelectric effect. We take into account the standard background model (B_0) (as considered in [1, 2]) and carry out a likelihood analysis to fit the DM induced signal, originating from the DM decays (i.e., $\chi \rightarrow \gamma\nu$) within the XENON1T detector, against the ER data [1, 2]. The resulting best-fit values of the DM decay width Γ and the corresponding 95% confidence level (C.L.) band are obtained as functions of the DM mass m_χ which varies in the range 2 – 60 keV. For illustration, a similar analysis is performed for two other background models, studied in [27], and in each case the corresponding constraints on the DM parameter space are derived.

In addition, decays of DM particles χ in galactic and extra-galactic sources produce X-ray photons which can be detected in various space-based X-ray telescopes such as Chandra, NuSTAR, XMM-Newton, HEAO-1 etc. Non-detections of any new signal in these experiments result in the upper limits in the $\Gamma - m_\chi$ plane [40–46], among which, Chandra and NuSTAR observations provide the strongest constraints. Simultaneously, the constraint coming from the CMB observation of Planck has also been taken into consideration [47, 48]. We compare our results with the aforementioned observational constraints and show that, for the standard background

* koushik@iiserkol.ac.in

† avirupghosh@hri.res.in

‡ arpankar@hri.res.in

§ biswarup@iiserkol.ac.in

model B_0 , some parts of the DM parameter space in the 95% C.L. region, obtained by fitting the XENON1T data, are consistent with all astrophysical observations. In case of the two additional backgrounds, too, substantial portions of the DM parameter space in the 95% C.L. bands are allowed by all observations.

The paper is organized as follows : In Sec. II, we discuss the DM model, backgrounds and corresponding analysis methodology. In Sec. III, we list up the possible astrophysical and cosmological observations that can constrain the parameter space of keV DM. In Sec. IV, we present our results and compare them with the observational constraints. We finally conclude in Sec. V.

II. MODEL AND ANALYSIS

In order to see the implications of the recently observed XENON1T electronic recoil (ER) data on a new physics signal, we consider a scenario consisting of a fermionic dark matter (DM) χ , decaying into a SM neutrino (ν) and a photon (γ). If the DM rest mass (m_χ) is in the range $\mathcal{O}(\text{keV})$ (as considered in this work), the corresponding energy of the produced photon will be $E_\gamma \simeq m_\chi/2$ (neglecting the ν mass which is in the sub-eV range).

It is conceivable that the DM particles present in our local galactic halo decay inside the cylindrical time projection chamber (TPC) of XENON1T detector which has a dimension $\sim 1\text{m} \times 1\text{m}$ [49]. The photons produced in such decays interact with the electrons of the xenon (Xe) atoms via photoelectric effect and contribute to the ER events observed in XENON1T. If one neglects the $\mathcal{O}(\text{eV})$ ionization energy of Xe, the corresponding recoiled electron energy spectrum is a monoenergetic peak at the photon energy $E_\gamma (\simeq m_\chi/2)$ [1] with the event rate (\mathcal{R}) given by

$$\mathcal{R} = \frac{1}{A} \left(\Gamma \frac{\rho_\odot^{\text{DM}}}{m_\chi} \langle L \rangle \right) \sigma_{\text{pe}}, \quad (1)$$

where $\rho_\odot^{\text{DM}} = 0.3$ (in GeVcm^{-3}) is the local energy density of DM particle χ (assuming χ accounts for the entire observed DM energy density) [50], m_χ is the DM mass (in keV) and Γ is the DM decay width (in s^{-1}). The quantities A ($\approx 131\text{u}$) and σ_{pe} (in b) denote the average atomic mass and the photoelectric cross-section of a Xe atom [51, 52], respectively. The ratio $\rho_\odot^{\text{DM}}/m_\chi$ signifies the local number density of DM particles. Photons produced from their decays over the average length scale $\langle L \rangle$ are capable of interacting with the Xe atoms, where $\langle L \rangle$ (in m) is the mean chord-length of the cylindrical TPC of XENON1T. The TPC is considered to be a cylinder of length 1m and diameter 1m [49] for which we found $\langle L \rangle \simeq 0.7\text{m}$ [53]. The quantity inside the parenthesis in Eq. 1 signifies the flux of the photons produced from the DM decays within the XENON1T TPC. In order to compare the event rate \mathcal{R} (given in Eq. 1) with that provided by the XENON1T collaboration [1, 2], we have to perform several unit conversions associated with m_χ (keV

to GeV), Γ (s^{-1} to yr^{-1}), $\langle L \rangle$ (m to cm) and σ_{pe} (b to cm^2). Additionally, we also need to include the conversion factor required to express u^{-1} in terms of t^{-1} . One thus ultimately obtains

$$\mathcal{R} (\text{t}^{-1}\text{y}^{-1}) = \frac{1.9 \times 10^{21}}{A} \Gamma \frac{\rho_\odot^{\text{DM}}}{m_\chi} \langle L \rangle \sigma_{\text{pe}}, \quad (2)$$

where the factor 1.9×10^{21} is arising from the unit conversions mentioned above.

In principle, decays of DM outside the XENON1T chamber can also impart energy to the electrons of the Xe atoms. However, the photon in such cases gets mostly shielded. On the other hand, neutrinos produced in these decays may enter into the detector and lead to electronic recoils via weak interaction. We have verified that such effects are down by several orders of magnitude, compared to what DM decays within the detector can do with the help of photons.

In order to obtain the recoiled electron energy spectrum as seen in XENON1T, we convolute the event rate given in Eq. 2 with a Gaussian distribution with energy resolution

$$\sigma(E) = a\sqrt{E} + bE, \quad (3)$$

where $a = 0.31 \sqrt{\text{keV}}$, $b = 0.0037$ [1] and E (in keV) is the energy of the recoiled electron. We have also included the effect of total detector efficiency [1] in our calculation.

The primary ER background used in our analysis is the standard background B_0 considered by the XENON1T collaboration [1, 2]:

B_0 : B_0 , consisting of ten distinct background components, represents the most widely used background model employed to fit the ER data recorded by the XENON1T experiment [1, 2]. The β -decays of ^{214}Pb and ^{85}Kr lead to continuous ER event distributions which give most dominant contributions to B_0 . In addition, monoenergetic peaks coming from the decays of $^{131\text{m}}\text{Xe}$, ^{125}I and $^{83\text{m}}\text{Kr}$ are also included along with several other continuous backgrounds [1].

Additionally, in order to demonstrate how our results vary with the choices of the background models, we have taken the following backgrounds into account ¹:

1. **PDF+³H:** Presence of tritium (^3H) within the Xe detector volume can be attributed to the cosmogenic activation of Xe as well as to the atmospheric abundances of tritiated water (HTO) and hydrogen (HT). Though, ^3H abundances originating from cosmogenic activation of Xe and from HTO appear to be negligible, the concentration of HT has

¹ Whether such backgrounds indeed contribute to the XENON1T ER data will be ultimately decided by future studies.

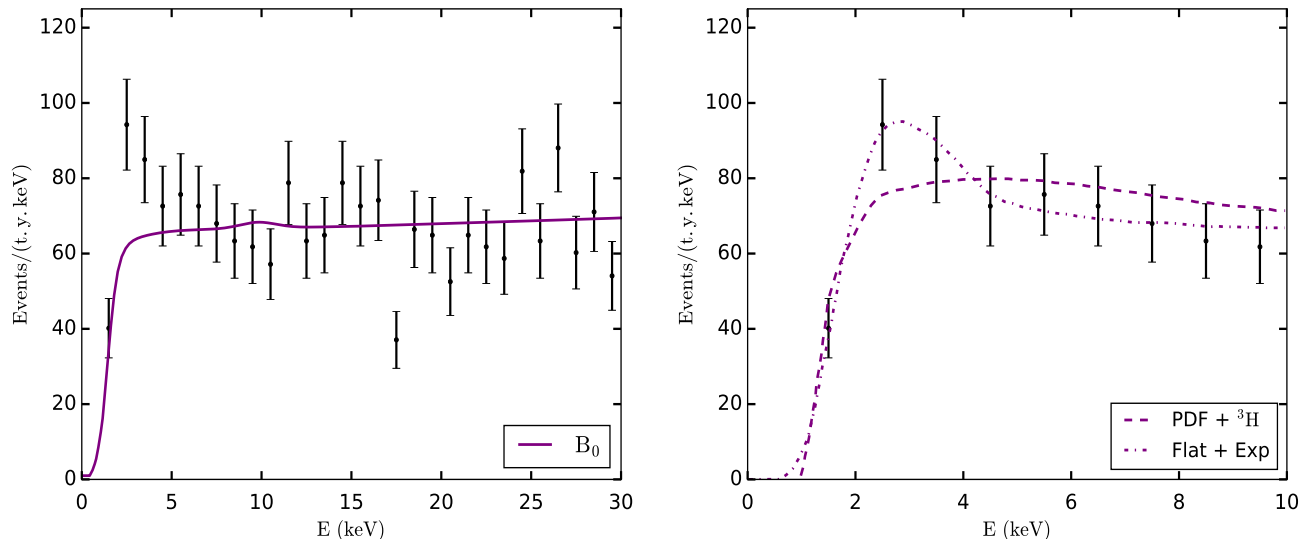


FIG. 1. *Left*: The best-fit ER event distribution for the standard background B_0 (obtained by the XENON1T collaboration in Refs. [1, 2]) is shown by the purple solid line. *Right*: In case of the two additional backgrounds PDF+ ^3H and Flat+Exp, the corresponding best-fit ER event distributions (as available in [27]) are represented by purple dashed and purple dash-dotted lines, respectively. In both of the panels, the XENON1T ER data, along with the associated 1σ error bars, are shown in black [1, 2].

substantial uncertainty. Furthermore, the uncertainties associated with the solubility and diffusion properties of ^3H within the Xe detector material and also the possibilities that tritium may form molecules other than HTO and HT make it difficult to rule out ^3H as a possible background component [1]. In our case, PDF + ^3H refers to the background model where the ER event distribution resulting from the β -decay of ^3H is added to that of the background mimicking B_0 (PDF) [1, 2, 27]. The background PDF, considered in our study, is the sum of all the components contributing to B_0 , but with a slightly different energy resolution [27], caused by the use of a simulation technique different than that used by the XENON1T collaboration [1].

2. **Flat+Exp**: Flat+Exp depicts a background model where a low energy exponential ER distribution is added to a flat ER distribution [27]. This background is purely a theoretical one without any known physical source but fits the data well (see [27] for details).

For our primary background B_0 as well as for the two additional backgrounds, we have considered the best-fit background rates which are shown in left and right panels of Fig. 1, respectively. These best-fit rates are obtained by fitting the corresponding backgrounds against the XENON1T data; see [1] and [27] for the details of the

analyses ². We then do a binned χ^2 analysis of the observed XENON1T data [1, 2] with our DM induced signal added to the best-fit rate of each of the above-mentioned backgrounds [1, 2, 27]. The χ^2 is defined as follows:

$$\chi^2(\Gamma, m_\chi) = \sum_i \frac{(n_{\text{data}}^i - n_{\text{exp}}^i)^2}{\sigma_i^2}, \quad (4)$$

where i signifies the energy bin, n_{data}^i is the data observed in the i th bin and σ_i is the associated error [1, 2]. n_{exp}^i is the expected number of events in the i th bin and is defined as $n_{\text{exp}}^i = n_{\text{background}}^i + n_{\text{signal}}^i(\Gamma, m_\chi)$. Here $n_{\text{background}}^i$ represents the best-fit background rate for a particular background, as discussed earlier. In case of the background B_0 , the best-fit rate in [1, 2] is provided for recoiled electron energy in the range between 1 keV and ~ 30 keV and hence the likelihood analysis is also carried out over the same energy range, i.e., first 29 bins of the XENON1T ER data [1, 2]. Due to this reason, the DM mass m_χ (which is twice the energy of the produced photon) is varied over the range 2–60 keV. On the other hand, for the background models PDF+ ^3H and Flat+Exp, the best-fit rates are available up to ~ 9 keV [27], and thus we have performed the χ^2 analysis in these cases over the energy range 1 keV to ~ 9 keV (first 9 bins) which well encloses the region of the reported excess, i.e., 2–3 keV [1, 2]. The DM mass m_χ , in these

² Only the best-fit rates of each of the backgrounds are available in [1, 2] and [27].

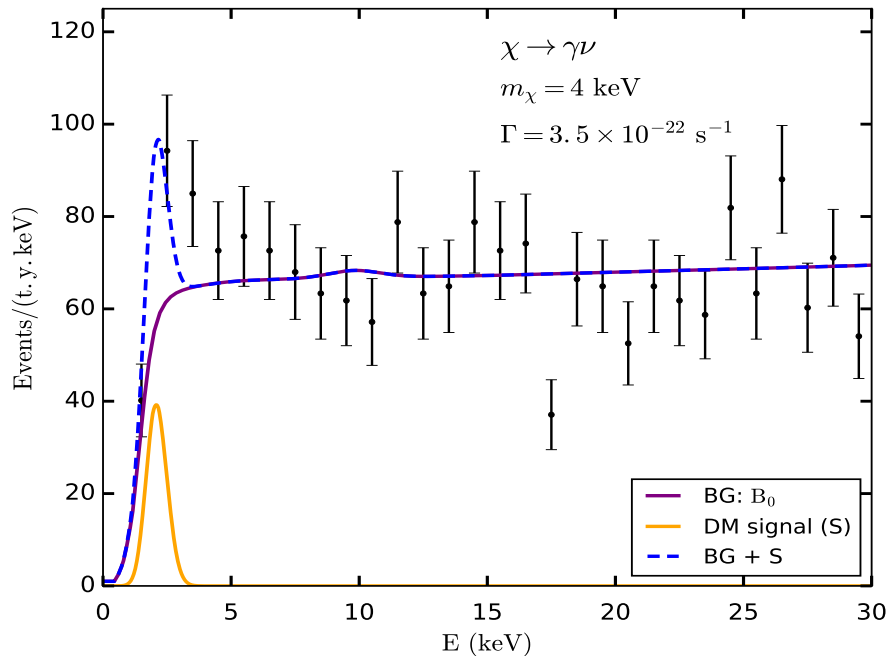


FIG. 2. The best-fit event distribution for a DM mass $m_\chi = 4$ keV, considering the standard background B_0 , has been shown as a function of the recoiled electron energy E (blue dashed curve). The background (BG) distribution (as given in [1, 2]) and the best-fit signal rate S (taking the effects of Gaussian smearing and detector efficiency into account) are shown by the purple and the orange solid lines, respectively. The XENON1T ER data (along with the error bars) are shown in black [1, 2].

cases, varies in the range 2 – 18 keV. Following [26], for each of the three background models, we have done the χ^2 minimization over the parameter Γ for a DM mass m_χ in the above-mentioned ranges and found the χ^2_{\min} which corresponds to the best-fit decay width. The 95% confidence level (C.L.) upper and lower limits on the DM decay width are obtained from:

$$\chi^2 = \chi^2_{\min} + 2.71. \quad (5)$$

In a single parameter fit in terms of Γ (for any m_χ), the above 95% C.L. range on both sides of χ^2_{\min} should yield the corresponding upper and lower limits on Γ .

III. ASTROPHYSICAL AND COSMOLOGICAL CONSTRAINTS

The DM χ populates the galaxies, galaxy clusters as well as the extra-galactic continuum. Since the DM mass is in the $\mathcal{O}(\text{keV})$ range, the monochromatic X-ray photons produced in the decays (i.e., $\chi \rightarrow \gamma\nu$) of such DM populations are possible to be observed in X-ray telescopes, e.g., XMM-Newton [54], Chandra [55, 56], HEAO-1 [57, 58], NuSTAR [59–62]. The non-observations of any line like feature in such experiments put constraints in the $\Gamma - m_\chi$ plane. For any given m_χ , the flux of X-ray photons, originating from the DM decay, is directly proportional to the DM decay width

Γ , i.e., larger the decay width is, greater the amount of the expected flux. Therefore, by comparing the observed flux with the flux expected from a decaying Γ of a particular mass, one obtains the upper limit on Γ and any higher value of Γ is thus ruled out for that particular DM mass. For example, one can use the XMM observation of X-ray flux from dwarf spheroidal (dSph) galaxies [44] to derive upper limits on Γ . We checked that, among all the dSphs observed by XMM, Carina gives the strongest bounds on Γ . The corresponding J-factor (in the field-of-view of XMM) for this dSph has been extracted from [63]. In parallel, the observations of Andromeda (M31) galaxy by Chandra [40] and NuSTAR [43], Milky Way (MW) galaxy by Chandra [41], Galactic Center (GC) by NuSTAR [42], diffuse cosmic hard X-Ray by HEAO-1 [46] and diffuse X-ray background by XMM and HEAO-1 [45] also constrain the parameter space of keV DM χ . Furthermore, the decay of χ during the reionization epoch can affect the cosmic microwave background (CMB) power spectrum. The observations of CMB temperature and polarization spectra by Planck [47] are used to derive upper limits on Γ [48]. It turns out that the observations of Chandra and NuSTAR provide the most stringent upper bounds on Γ , so far.

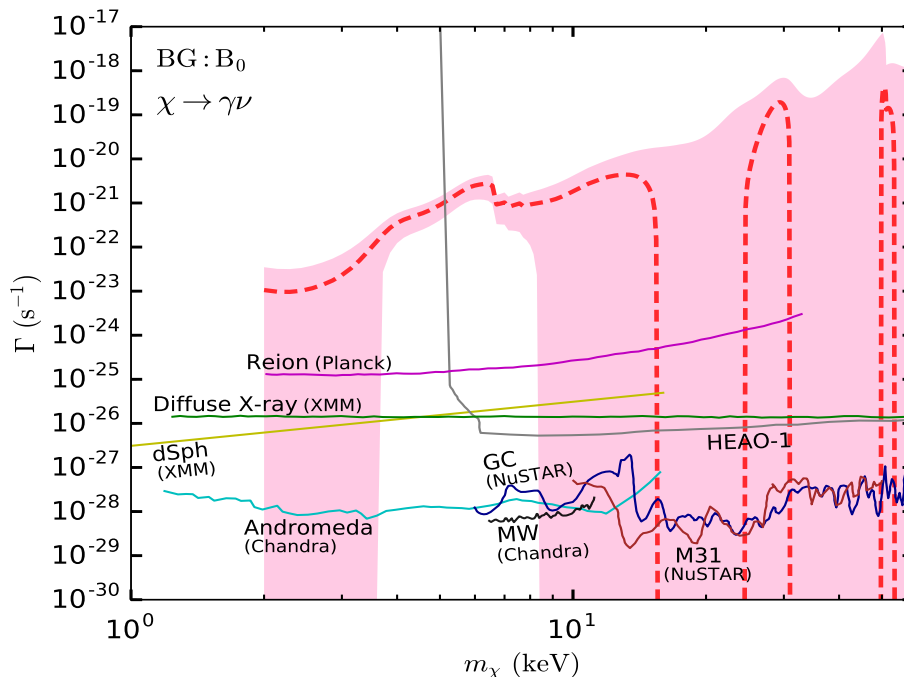


FIG. 3. The best-fit DM decay width (red dashed line) and the region enclosed by the 95% C.L. upper and lower limits (pink shaded region), obtained by fitting the XENON1T data [1, 2], have been shown as functions of the DM mass m_χ , considering the background (BG) model B_0 [1, 2]. The solid lines represent the upper limits coming from various X-ray observations, e.g., XMM observation of dSph Carina (yellow) [44], HEAO-1 observation of hard diffuse X-ray background (gray) [46, 58], XMM and HEAO-1 observations of diffuse X-ray background (green) [45], Chandra observations of Andromeda (cyan) [40] and Milky Way (MW) (black) [41] galaxies, NuSTAR observations of Galactic Cente (GC) (blue) [42] and Andromeda (M31) (brown) [43] and Planck observation of the CMB spectrum (magenta) [47, 48] (see the text for details).

IV. RESULTS

Fig. 2 shows the best-fit electron recoil energy distribution (as a function of the electron energy E) for a DM mass $m_\chi = 4$ keV, considering the background model B_0 . In this case, following Eq. 4, one obtains the best-fit DM decay width $\Gamma = 3.5 \times 10^{-22} \text{ s}^{-1}$. The orange solid line, centered around $E \simeq m_\chi/2 = 2$ keV, represents the corresponding signal event distribution S (incorporating the effects of Gaussian smearing and detector efficiency), while the purple solid line is the event distribution for the B_0 background (taken from [1, 2]). The blue dashed curve corresponds to the total event distribution obtained by adding the signal event distribution (S) to the background B_0 . It can be seen from this figure, while B_0 fits the data well in the higher energy bins, substantial contributions from some new physics scenarios (for example, dark matter), are required to match the data in the lower energy bins where the actual excess was observed.

Fig. 3 represents the constraints on the DM decay width (Γ), obtained by fitting the XENON1T data, for DM mass m_χ in the range 2 – 60 keV, considering the background model B_0 . In addition to the best-fit Γ (dashed line), the area enclosed by the 95% C.L. upper and lower limits (shaded region) is also shown. In the energy range $1.75 \text{ keV} \lesssim E \lesssim 4.25 \text{ keV}$, the back-

ground B_0 is much lower than the observed excess, even after considering the associated 2σ uncertainty (see left panel of Fig. 1 and Fig. 2) and hence, in order to match the data in this energy region, the required DM decay width (i.e., the full 95% C.L. band) becomes large for DM masses in the range 3.5 – 8.5 keV. Outside this energy region, B_0 always lies within the 2σ error bars of the data (see Fig. 1; left panel and also Fig. 2). As a result, the 95% C.L. lower limit on Γ is zero for $2 \text{ keV} \lesssim m_\chi \lesssim 3.5 \text{ keV}$ and $8.5 \text{ keV} \lesssim m_\chi \lesssim 60 \text{ keV}$. The best-fit Γ , on the other hand, is zero only for the DM mass ranges $15 \text{ keV} \lesssim m_\chi \lesssim 24 \text{ keV}$, $31 \text{ keV} \lesssim m_\chi \lesssim 50 \text{ keV}$ and $54 \text{ keV} \lesssim m_\chi \lesssim 60 \text{ keV}$, since B_0 fits the data quite well in the corresponding energy domains (see Fig. 1; left panel and Fig. 2), leaving little scope for adding any new signal. However, if one thinks in terms of the full 2σ uncertainty of the XENON1T data, some scope still remains for adding new physics signals. This fact is reflected in the large value of the 95% C.L. upper limit on Γ throughout the DM mass range 2 – 60 keV.

In Fig. 3, together with the limits obtained from the XENON1T data considering B_0 as the background model, we have also shown the astrophysical and cosmological constraints on Γ , discussed in Sec. III, by various solid lines. The yellow solid line in Fig. 3 represents the 95% C.L. upper limit on Γ , coming from the XMM ob-

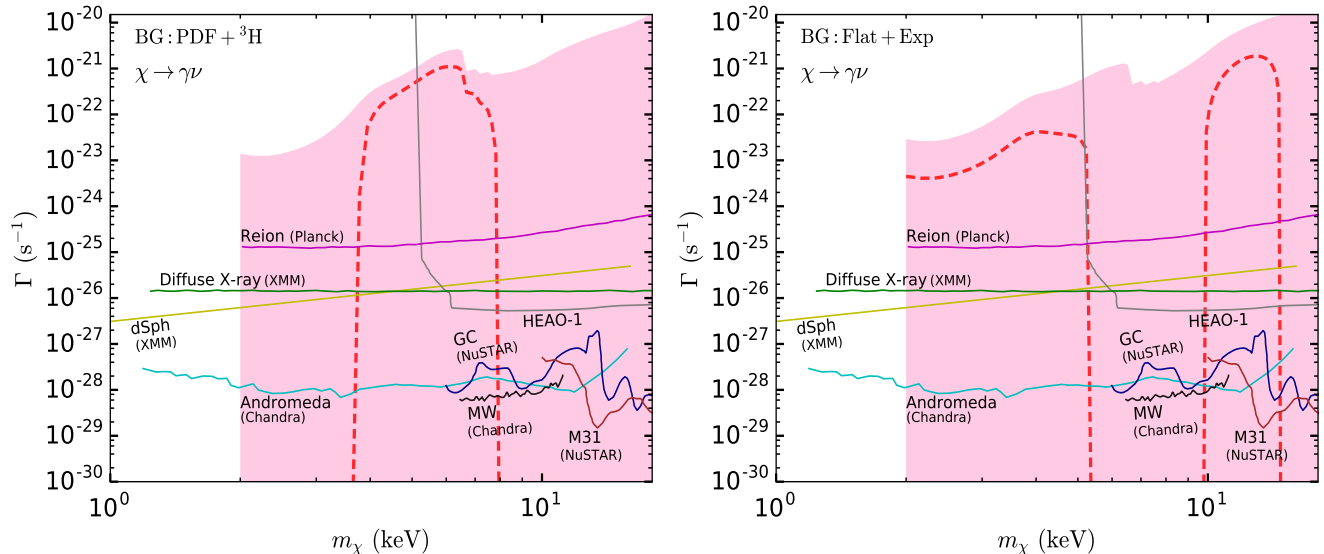


FIG. 4. The best-fit Γ 's (red dashed lines) and the associated 95% C.L. bands (pink shaded regions), resulting from the analysis of the XENON1T data [1, 2], are presented as functions of m_χ , taking into account the background (BG) models PDF+ ^3H (left panel) [27] and Flat+Exp (right panel) [27]. The astrophysical and cosmological constraints, shown in each panel, are same as in Fig. 3 (see the text for details).

observation of dSph Carina [44]. The upper limits from the observations of diffuse X-ray background by XMM and HEAO-1 (at 95% C.L.) [45], Andromeda (M31) galaxy by Chandra (at 95% C.L.) [40] and NuSTAR (at 95% C.L.) [43], diffuse cosmic hard X-Ray by HEAO-1 (at 95% C.L.) [46, 58], Milky Way (MW) galaxy by Chandra (at 99% C.L.) [41], Galactic Center (GC) by NuSTAR (at 95% C.L.) [42] are shown by green, cyan, brown, gray, black and blue solid lines, respectively. The Planck CMB constraint on Γ (at 95% C.L.) has been shown in Fig. 3 by magenta solid line [48]. As mentioned earlier, the Chandra observations of Andromeda and Milky Way (MW) galaxies as well as the NuSTAR observations of Andromeda (M31) and Galactic Center (GC) put the tightest constraints in the $\Gamma - m_\chi$ plane.

It can be seen from Fig. 3 that for the background model B_0 , the 95% C.L. upper limit on Γ , obtained by analyzing the XENON1T data, is ruled out by X-ray observations as well as by Planck CMB observation over the mass range 2 – 60 keV. However, if one considers the full 95% C.L. band associated with the best-fit Γ , there still exist some scopes to allow the DM induced signals. For example, since the 95% C.L. lower limit on Γ is zero for $2 \text{ keV} \lesssim m_\chi \lesssim 3.5 \text{ keV}$ and $8.5 \text{ keV} \lesssim m_\chi \lesssim 60 \text{ keV}$, any finite Γ in these mass ranges which is lower than all the astrophysical constraints is allowed at 95% C.L. On the other hand, for DM masses in the range $3.5 \text{ keV} \lesssim m_\chi \lesssim 8.5 \text{ keV}$, the full 95% C.L. band is disfavoured.

The best-fit Γ 's and the associated 95% C.L. bands, resulting from the analysis of the XENON1T data using background models PDF+ ^3H and Flat+Exp are shown in left and right panels of Fig. 4, respectively. Both of these backgrounds are well inside the 2σ error bars of

the XENON1T data in all energy bins (see Fig. 1; right panel) and thus, in each case, the 95% C.L. lower limit on Γ is zero over the entire DM mass range considered, i.e., 2 – 18 keV. Although the 95% C.L. lower limits on Γ , for these two backgrounds, show similar behaviour throughout the mass domain 2 – 18 keV, the best-fit Γ 's are significantly different. For the PDF+ ^3H background, the best-fit $\Gamma = 0$ for $2 \text{ keV} \lesssim m_\chi \lesssim 3.5 \text{ keV}$ and $8 \text{ keV} \lesssim m_\chi \lesssim 18 \text{ keV}$, while it is relatively larger for other DM masses because the background falls below the data in the corresponding energy regions (see right panel of Fig. 1). In case of Flat+Exp background, the best-fit Γ is zero for $5 \text{ keV} \lesssim m_\chi \lesssim 10 \text{ keV}$ and $15 \text{ keV} \lesssim m_\chi \lesssim 18 \text{ keV}$, since this background fits the data well in the energy ranges $2.5 \text{ keV} \lesssim E \lesssim 5 \text{ keV}$ and $7.5 \text{ keV} \lesssim E \lesssim 9 \text{ keV}$ (see Fig. 1; right panel). Like in the case of B_0 , for PDF+ ^3H and Flat+Exp backgrounds, too, the 95% C.L. upper limits on Γ are large for all DM masses in the range 2 – 18 keV. Along with the XENON1T results, similar astrophysical and cosmological constraints, shown in Fig. 3, are also presented in each panel of Fig. 4. By comparing these constraints with those obtained from the analysis of the XENON1T data, one finds that, though the 95% C.L. upper limits on Γ are always ruled out for both of the background models, in each case, a significant portion of the DM parameter space in the 95% C.L. region, which is consistent with all the astrophysical observations, exists for all DM masses in the range 2 – 18 keV. This observation is in contrast to what has been seen in the case of B_0 .

The local DM density ρ_\odot^{DM} is an important quantity in determining the ER event rate in the XENON1T experiment (see Eq. 1 and Eq. 2). In this study we have

considered the local DM density ρ_{\odot}^{DM} to be fixed at its central value 0.3 GeVcm^{-3} [50]. If one considers the full 1σ range of $\rho_{\odot}^{\text{DM}} = 0.2 - 0.4 \text{ GeVcm}^{-3}$ [50], all finite constraints on Γ (both the best-fit and the 95% C.L.) will vary by a factor of $0.7 - 1.3$, i.e., within 30% of the values presented here.

V. SUMMARY AND CONCLUSIONS

We have studied, in the context of the recent XENON1T observation, a fermionic keV DM scenario where the DM particle χ decays into a photon and a SM neutrino. Photons produced in the decay of local population of these DM particles inside the XENON1T chamber are absorbed by the electrons of the Xe atoms and thereby contribute to the recoiled electron events recorded by XENON1T. We have primarily considered the standard background B_0 [1, 2] for our study. By adding B_0 to the DM induced signal and performing an one parameter χ^2 analysis against the XENON1T data, we have obtained the best-fit values of the DM decay width Γ and the associated 95% C.L. band as functions of the DM mass m_{χ} in the range $2 - 60 \text{ keV}$. In addition, two other background models, namely, PDF+ ^3H [27] and Flat+Exp [27] are also taken into account, for the sake of illustration. Although PDF+ ^3H has substantial uncertainty associated with it and Flat+Exp is purely speculative, they provide comparatively better fit to the observed XENON1T excess. For both of these backgrounds, the corresponding best-fit Γ 's and the 95% C.L. bands are estimated for the DM mass range $2 - 18 \text{ keV}$, by carrying out an analysis similar to the case of B_0 .

On the other hand, photons produced in the decays of keV DM particles, occurring in the extra-galactic continuum and various astrophysical structures, are expected to be observed in X-ray observations. These keV DM particles can also decay during the reionization epoch and leave footprints in the CMB spectrum observed by Planck. Constraints coming from these observations in the $\Gamma - m_{\chi}$ plane have been taken into account and juxtaposed with the results obtained from the XENON1T data. We find that, the DM mass range $3.5 \text{ keV} \lesssim m_{\chi} \lesssim 8.5 \text{ keV}$ is strongly disfavoured at 95% C.L. by all astrophysical observations so long as the most commonly used background B_0 is considered to be the only reliable source of background. However, for DM masses outside the above-mentioned window (i.e., $2 \text{ keV} \lesssim m_{\chi} \lesssim 3.5 \text{ keV}$ and $8.5 \text{ keV} \lesssim m_{\chi} \lesssim 60 \text{ keV}$), substantial parts of the DM parameter space are still allowed at 95% C.L. Such

conclusions regarding the allowed regions in the DM parameter space depend on the energy distribution of the background model under consideration, a fact which is demonstrated by choosing the backgrounds PDF+ ^3H and Flat+Exp. In both of these cases, reasonable portions of the DM parameter space that lie within the 95% C.L. bands throughout the DM mass range $2 - 18 \text{ keV}$ are found to be consistent with all astrophysical data.

The results presented in Figs. 2, 3 and 4 can be appropriately translated in terms of the parameters of specific theoretical models, including those mentioned in the introduction. The R-parity violating gravitino DM scenario is in general quite constrained in this respect, since the ‘mixing parameter’ driving the DM decay is subjected to tight limits from neutrino masses on the one hand, and restrictions on the inter-connected particle spectrum on the other. The axino DM scenario is less restricted, being possessed with relatively larger number of phenomenological parameters.

As mentioned in the introduction, the constraints obtained from the XENON1T data as well as the X-ray observations etc., assume that the DM density of our universe is saturated by warm DM. For the m_{χ} -range of our interest, such saturation can be questionable if the constraints from the Lyman- α forest are imposed, as has been claimed, for example, in [64]. Higher values of Γ will be required in such cases, leading to some quantitative changes in all the constraints. For example, if a maximum fraction f of the relic density can be attributed to warm DM, then the limits on Γ from every considerations in Fig. 3 and in each panel of Fig. 4 get scaled up to Γ/f .

To conclude, the recent XENON1T data may be interpreted as the source of additional constraints on dark matter scenarios, the severity of the constraints being dependent on detailed understanding of the backgrounds. This become evident from the above study on otherwise allowed decaying warm dark matter.

ACKNOWLEDGMENTS

The authors thank Pijushpani Bhattacharjee and Subinoy Das for useful discussions. The work of KD was partially supported by the grant MTR/2019/000395, funded by SERB, DST, Government of India. The work of AG and AK was partially supported by funding available from the Department of Atomic Energy, Government of India, for the Regional Centre for Accelerator-based Particle Physics (RECAPP), Harish-Chandra Research Institute, Allahabad.

-
- [1] E. Aprile *et al.* (XENON), Phys. Rev. D **102**, 072004 (2020), arXiv:2006.09721 [hep-ex].
 [2] X. Collaboration, (2020), 10.5281/zenodo.4273099.
 [3] K. Kannike, M. Raidal, H. Veermäe, A. Strumia, and D. Teresi, Phys. Rev. D **102**, 095002 (2020),

- arXiv:2006.10735 [hep-ph].
 [4] F. Takahashi, M. Yamada, and W. Yin, Phys. Rev. Lett. **125**, 161801 (2020), arXiv:2006.10035 [hep-ph].
 [5] G. Alonso-Álvarez, F. Ertas, J. Jaeckel, F. Kahlhoefer, and L. J. Thormaehlen, JCAP **11**, 029 (2020),

- arXiv:2006.11243 [hep-ph].
- [6] J. Buch, M. A. Buen-Abad, J. Fan, and J. S. C. Leung, *JCAP* **10**, 051 (2020), arXiv:2006.12488 [hep-ph].
- [7] K. Nakayama and Y. Tang, *Phys. Lett. B* **811**, 135977 (2020), arXiv:2006.13159 [hep-ph].
- [8] H. An, M. Pospelov, J. Pradler, and A. Ritz, *Phys. Rev. D* **102**, 115022 (2020), arXiv:2006.13929 [hep-ph].
- [9] I. M. Bloch, A. Caputo, R. Essig, D. Redigolo, M. Sholapurkar, and T. Volansky, (2020), arXiv:2006.14521 [hep-ph].
- [10] M. Lindner, Y. Mambrini, T. B. de Melo, and F. S. Queiroz, *Phys. Lett. B* **811**, 135972 (2020), arXiv:2006.14590 [hep-ph].
- [11] N. Okada, S. Okada, D. Raut, and Q. Shafi, *Phys. Lett. B* **810**, 135785 (2020), arXiv:2007.02898 [hep-ph].
- [12] P. Athron *et al.*, (2020), arXiv:2007.05517 [astro-ph.CO].
- [13] C. Gao, J. Liu, L.-T. Wang, X.-P. Wang, W. Xue, and Y.-M. Zhong, *Phys. Rev. Lett.* **125**, 131806 (2020), arXiv:2006.14598 [hep-ph].
- [14] J. B. Dent, B. Dutta, J. L. Newstead, and A. Thompson, *Phys. Rev. Lett.* **125**, 131805 (2020), arXiv:2006.15118 [hep-ph].
- [15] T. Li, (2020), arXiv:2007.00874 [hep-ph].
- [16] C. Cai, H. H. Zhang, M. T. Frandsen, M. Rosenlyst, and G. Cacciapaglia, *Phys. Rev. D* **102**, 075018 (2020), arXiv:2006.16267 [hep-ph].
- [17] S. Shakeri, F. Hajkarim, and S.-S. Xue, (2020), arXiv:2008.05029 [hep-ph].
- [18] I. M. Shoemaker, Y.-D. Tsai, and J. Wyenberg, (2020), arXiv:2007.05513 [hep-ph].
- [19] O. Miranda, D. Papoulias, M. Tórtola, and J. Valle, *Phys. Lett. B* **808**, 135685 (2020), arXiv:2007.01765 [hep-ph].
- [20] A. N. Khan, *Phys. Lett. B* **809**, 135782 (2020), arXiv:2006.12887 [hep-ph].
- [21] K. S. Babu, S. Jana, and M. Lindner, *JHEP* **10**, 040 (2020), arXiv:2007.04291 [hep-ph].
- [22] B. Fornal, P. Sandick, J. Shu, M. Su, and Y. Zhao, *Phys. Rev. Lett.* **125**, 161804 (2020), arXiv:2006.11264 [hep-ph].
- [23] A. Bally, S. Jana, and A. Trautner, *Phys. Rev. Lett.* **125**, 161802 (2020), arXiv:2006.11919 [hep-ph].
- [24] S. Xu and S. Zheng, (2020), arXiv:2012.10827 [hep-ph].
- [25] G. Choi, M. Suzuki, and T. T. Yanagida, *Phys. Lett. B* **811**, 135976 (2020), arXiv:2006.12348 [hep-ph].
- [26] B. Bhattacharjee and R. Sengupta, (2020), arXiv:2006.16172 [hep-ph].
- [27] M. Szydagis, C. Levy, G. Blockinger, A. Kamaha, N. Parveen, and G. Rischbieter, (2020), arXiv:2007.00528 [hep-ex].
- [28] A. E. Robinson, (2020), arXiv:2006.13278 [hep-ex].
- [29] T. Asaka and M. Shaposhnikov, *Phys. Lett. B* **620**, 17 (2005), arXiv:hep-ph/0505013.
- [30] T. Asaka, M. Laine, and M. Shaposhnikov, *JHEP* **01**, 091 (2007), [Erratum: *JHEP* **02**, 028 (2015)], arXiv:hep-ph/0612182.
- [31] F. Hofmann, J. S. Sanders, K. Nandra, N. Clerc, and M. Gaspari, *Astron. Astrophys.* **592**, A112 (2016), arXiv:1606.04091 [astro-ph.CO].
- [32] P. Dey, B. Mukhopadhyaya, S. Roy, and S. K. Vempati, *JCAP* **05**, 042 (2012), arXiv:1108.1368 [hep-ph].
- [33] F. Takayama and M. Yamaguchi, *Phys. Lett. B* **485**, 388 (2000), arXiv:hep-ph/0005214.
- [34] L. Covi and J. E. Kim, *New J. Phys.* **11**, 105003 (2009), arXiv:0902.0769 [astro-ph.CO].
- [35] J.-C. Park, S. C. Park, and K. Kong, *Phys. Lett. B* **733**, 217 (2014), arXiv:1403.1536 [hep-ph].
- [36] K.-Y. Choi and O. Seto, *Phys. Lett. B* **735**, 92 (2014), arXiv:1403.1782 [hep-ph].
- [37] G. F. Giudice and R. Rattazzi, *Phys. Rept.* **322**, 419 (1999), arXiv:hep-ph/9801271.
- [38] C. Kolda and J. Unwin, *Phys. Rev. D* **90**, 023535 (2014), arXiv:1403.5580 [hep-ph].
- [39] N. E. Bomark and L. Roszkowski, *Phys. Rev. D* **90**, 011701 (2014), arXiv:1403.6503 [hep-ph].
- [40] C. R. Watson, Z.-Y. Li, and N. K. Polley, *JCAP* **03**, 018 (2012), arXiv:1111.4217 [astro-ph.CO].
- [41] D. Sicilian, N. Cappelluti, E. Bulbul, F. Civano, M. Moschetti, and C. S. Reynolds, (2020), arXiv:2008.02283 [astro-ph.HE].
- [42] K. Perez, K. C. Y. Ng, J. F. Beacom, C. Hersh, S. Horiuchi, and R. Krivonos, *Phys. Rev. D* **95**, 123002 (2017), arXiv:1609.00667 [astro-ph.HE].
- [43] K. C. Ng, B. M. Roach, K. Perez, J. F. Beacom, S. Horiuchi, R. Krivonos, and D. R. Wik, *Phys. Rev. D* **99**, 083005 (2019), arXiv:1901.01262 [astro-ph.HE].
- [44] T. Jeltema and S. Profumo, *Astrophys. J.* **686**, 1045 (2008), arXiv:0805.1054 [astro-ph].
- [45] A. Boyarsky, A. Neronov, O. Ruchayskiy, and M. Shaposhnikov, *Mon. Not. Roy. Astron. Soc.* **370**, 213 (2006), arXiv:astro-ph/0512509.
- [46] R. Essig, E. Kuflik, S. D. McDermott, T. Volansky, and K. M. Zurek, *JHEP* **11**, 193 (2013), arXiv:1309.4091 [hep-ph].
- [47] P. Ade *et al.* (Planck), *Astron. Astrophys.* **594**, A13 (2016), arXiv:1502.01589 [astro-ph.CO].
- [48] I. M. Oldengott, D. Boriero, and D. J. Schwarz, *JCAP* **08**, 054 (2016), arXiv:1605.03928 [astro-ph.CO].
- [49] E. Aprile *et al.* (XENON), *Eur. Phys. J. C* **77**, 881 (2017), arXiv:1708.07051 [astro-ph.IM].
- [50] J. Bovy and S. Tremaine, *Astrophys. J.* **756**, 89 (2012), arXiv:1205.4033 [astro-ph.GA].
- [51] H. Hirayama, (2021).
- [52] E. Storm and H. I. Israel, 10.2172/4583232.
- [53] A. M. Kellerer, *Radiation Research* **47**, 359 (1971).
- [54] C. Arviset, M. Guainazzi, J. Hernandez, J. Dowson, P. Osuna, and A. Venet, (2002), arXiv:astro-ph/0206412.
- [55] M. Weisskopf, B. Brinkman, C. Canizares, G. Garmire, S. Murray, and L. Van Speybroeck, *Publ. Astron. Soc. Pac.* **114**, 1 (2002), arXiv:astro-ph/0110308.
- [56] I. N. E. *et al.*, **189**, 37 (2010).
- [57] F. E. Marshall, E. A. Boldt, S. S. Holt, R. B. Miller, R. F. Mushotzky, L. A. Rose, R. E. Rothschild, and P. J. Serlemitsos, *Astrophys. J.* **235**, 4 (1980).
- [58] D. Gruber, J. Matteson, L. Peterson, and G. Jung, *Astrophys. J.* **520**, 124 (1999), arXiv:astro-ph/9903492.
- [59] K. Mori *et al.*, *Astrophys. J.* **814**, 94 (2015), arXiv:1510.04631 [astro-ph.HE].
- [60] J. Hong *et al.*, *Astrophys. J.* **825**, 132 (2016), arXiv:1605.03882 [astro-ph.HE].
- [61] M. Lazzarini *et al.*, *Astrophys. J.* **862**, 28 (2018), arXiv:1806.03305 [astro-ph.HE].
- [62] H. Stiele and A. Kong, *Mon. Not. Roy. Astron. Soc.* **475**, 4911 (2018), arXiv:1801.10151 [astro-ph.HE].
- [63] A. Geringer-Sameth, S. M. Koushiappas, and M. Walker, *Astrophys. J.* **801**, 74 (2015), arXiv:1408.0002 [astro-ph.CO].

- [64] V. Iršič *et al.*, Phys. Rev. D **96**, 023522 (2017),
arXiv:1702.01764 [astro-ph.CO].